Spatiotemporal distribution and morphological diversity of the Cambrian *Wiwaxia*: New insights from South China

Haijing Sun [a,b], Fangchen Zhao [a,b,*], Ruolin Wu [c], Han Zeng [a,b], Zhixin Sun [a,b]

[a] *State Key Laboratory of Palaeobiology and Stratigraphy, Nanjing Institute of Geology and Palaeontology, Chinese Academy of Sciences, Nanjing 210008, China*
[b] *College of Earth and Planetary Sciences, University of Chinese Academy of Sciences, Beijing 100049, China*
[c] *Bristol Palaeontology Group, School of Earth Sciences, Universality of Bristol, Bristol BS8 1TQ, UK*

A B S T R A C T

Wiwaxia is a well-known Cambrian animal and a relative of annelids and molluscs, characterized by its densely arranged, imbricated dorsal sclerites. Despite its prevalence in the fossil record, the scarcity of articulated specimens leading to persistent uncertainties regarding its morphological diversities and evolutionary history has fueled ongoing investigations. This study presents an additional articulated specimen and isolated sclerites from the Cambrian Stage 4 Douposi Formation in Yunnan Province, South China, representing a new species—*Wiwaxia douposiensis* sp. nov. The newly described materials, originating from a new Cambrian Konservat-Lagerstätte, exhibit typical Burgess Shale-type preservation. They unveil a distinctive two-order rib pattern and aspect ratios of sclerites. The temporal and spatial distribution of *Wiwaxia* suggests a potential origination centered in South China during the Cambrian Age 3, with an expanding pattern from shallow to deep waters and from warm-humid to dry-cold climates during the Cambrian Age 4 to Drumian. Statistical and phylogenetic analyses highlight the dual aspects of conservative aspect ratios in sclerites, and morphological variations observed at the species levels within *Wiwaxia*.

1. Introduction

Wiwaxia, an organism resembling a slug, thrived globally during the Cambrian Epoch 2–Miaolingian. This taxon is distinguished by a dense dorsal covering of non-biomineralized, imbricated sclerites arranged in five zones (ventro-lateral, lower-lateral, upper-lateral, dorsal and anterior) and a series of transverse rows across the body. Each sclerite was attached to the body wall via a prominent root (Conway Morris, 1985), the morphology of which varies depending on zone membership (Conway Morris, 1985; Smith, 2014). Dorsal spines began to develop in the type species *W. corrugata* once the body length reaches 8–16 mm (Smith, 2014), and functioned as defensive armors (Conway Morris, 1985). Sclerites of *Wiwaxia* periodically sloughed off and were replaced by new, larger ones with slight sclerite morphological modifications during their ontogeny (Bengtson and Conway Morris, 1984; Conway Morris, 1985). The peculiar appearance of *Wiwaxia* has intrigued palaeontologists for decades to unravel their evolutionary mysteries.

The sclerite character, involving microvilli secretion and forming a distinctively striated internal microstructure, classifies *Wiwaxia* within the lophotrochozoan total group (Butterfield, 1990). However, its precise phylogenetic position has long been a subject of controversy. The main debate surrounded whether *Wiwaxia* belonged to polychaete annelids based on sclerite structure and histology (Butterfield, 1990; Butterfield, 2006), or to molluscs based on radula and creeping foot (Caron et al., 2006; Smith, 2012, 2014). More recent investigations have assigned *Wiwaxia* to the stem group of annelids+molluscs (Zhang et al., 2015). Despite its classification, *Wiwaxia* was likely a close relative of either molluscs, annelids, or their last common ancestor, making it a valuable proxy for the last common ancestor(s) of Annelida and Mollusca.

Articulated specimens play a crucial role in comprehending the biological, ecological, and phylogenetic aspects of *Wiwaxia*, yet they are rare in the fossil record, having been unearthed from only six localities in South China (Zhao, 2011; Yang et al., 2014; Zhang et al., 2015), Laurentia (Conway Morris, 1985; Conway Morris et al., 2015), and Siberia (Ivantsov et al., 2005a). There is also a potential presence in Australia (Porter, 2004, p.588), although the relevant material has not yet been published. Here we report a new species, *Wiwaxia douposiensis*

sp. nov., identified from an articulated *Wiwaxia* specimen and several isolated sclerites from the Douposi Formation (Cambrian Stage 4), Yunnan Province, South China. The materials uncovered contribute novel insights into morphological variations and taphonomic characteristics. Additionally, we provide a summary of the spatiotemporal distributions, as well as the diversity of *Wiwaxia*, shedding new light on its dispersal history and morphological plasticity.

2. Geological setting

The Douposi Formation is well exposed in East Yunnan, South China, exhibiting a thickness ranging from 3 to 120 m (Luo et al., 1993). Deposited in subtidal to tidal flat environments (Xiang et al., 1999), this succession is characterized by fine-grained siliciclastic sediments and carbonates. It conformably overlies the Shanyicun Formation and underlies the Shuanglongtan Formation. Stratigraphically, it spans the boundary between the Cambrian Series 2 and Miaolingian (Luo et al.,
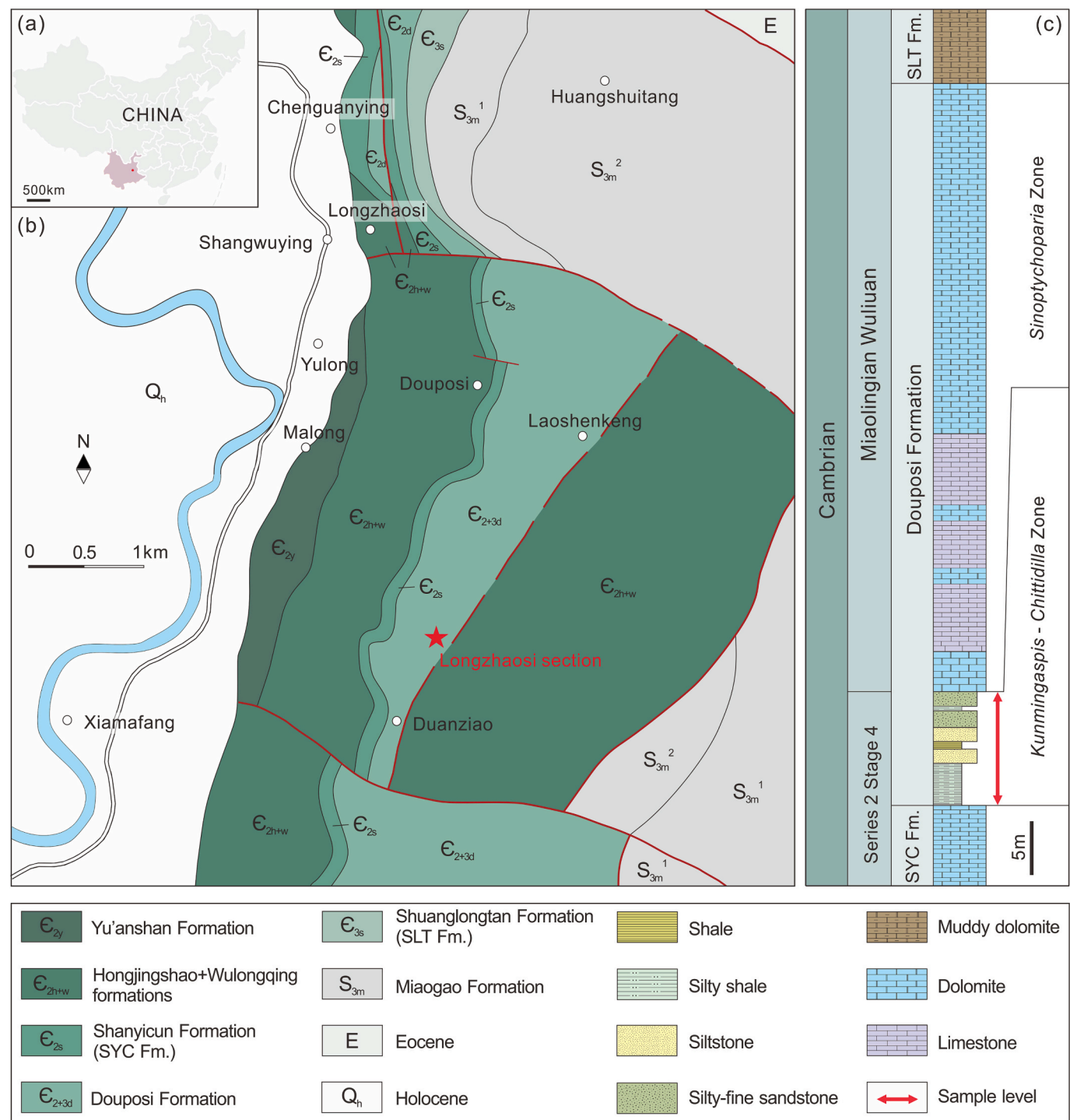

Fig. 1. (**a**) Location of Yunnan Province in China. (**b**) Geological map of the Yiliang area, and the red star indicating the location of Longzhaosi section (modified from Luo et al., 1993). (**c**) Lithostratigraphic column of the Douposi Formation at Longzhaosi section and the sampling level. (For interpretation of the references to colour in this figure legend, the reader is referred to the web version of this article.)

1993; Peng, 2020). Two trilobite biozones within the Douposi Formation have been identified: the lower *Kunmingaspis–Chittidilla* Zone (Cambrian Stage 4) and the Upper *Sinoptuchoparia* Zone (Cambrian Wuliuian).

The examined Douposi Formation in the Longzhaosi section, situated near Longzhaosi in Yiliang County, the eastern part of Yunnan Province (N 24°49′6.7512″, E 103°11′53.592″; Fig. 1a, b), was initially described and measured by Luo et al. (1993). This sequence, 59 m thick, comprises two lithologic members: the Lower Member, dominated by yellow to yellowish-green shales, siltstones, and fine-grained sandstones; the Upper Member, characterized by greyish thin-bedded limestones and dolostones (Fig. 1a). *Wiwaxia* specimens were collected from the lower siliciclastic Member of the Douposi Formation, and trilobites from the same interval indicates the *Kunmingaspis − Chittidilla* Zone (Fig. 2a, b). The *Wiwaxia*-bearing interval also yields algae (Fig. 2c), abundant trace fossils (e.g. Fig. 2d), articulated brachiopods (Fig. 2e, h) with soft parts

including visceral organs (Fig. 2f), setae (Fig. 2g) and a possible pedicle (Fig. 2h), *Scenella* (Fig. 2i), echinoderms (Fig. 2j), a diverse array of non-trilobite arthropods (e.g. Fig. 2k), a ventulicoliid with soft organs (Fig. 2l), tubular worms (Fig. 2m), and other problematic organisms with uncertain affinity. This new assemblage represents a Burgess Shale-type Lagerstätte, warranting further exploration and research.

3. Material and methods

Fourteen specimens of *Wiwaxia* were available, including one articulated specimen with its part and counterpart slabs, while the remaining specimens consisted of isolated sclerites. All fossil specimens described in this study are curated at the Nanjing Institute of Geology and Palaeontology, Chinese Academy of Sciences (NIGPAS).

Examinations and photographs were conducted using a standard light microscope (Zeiss Stemi 508), a Carl Zeiss SteREO Discovery
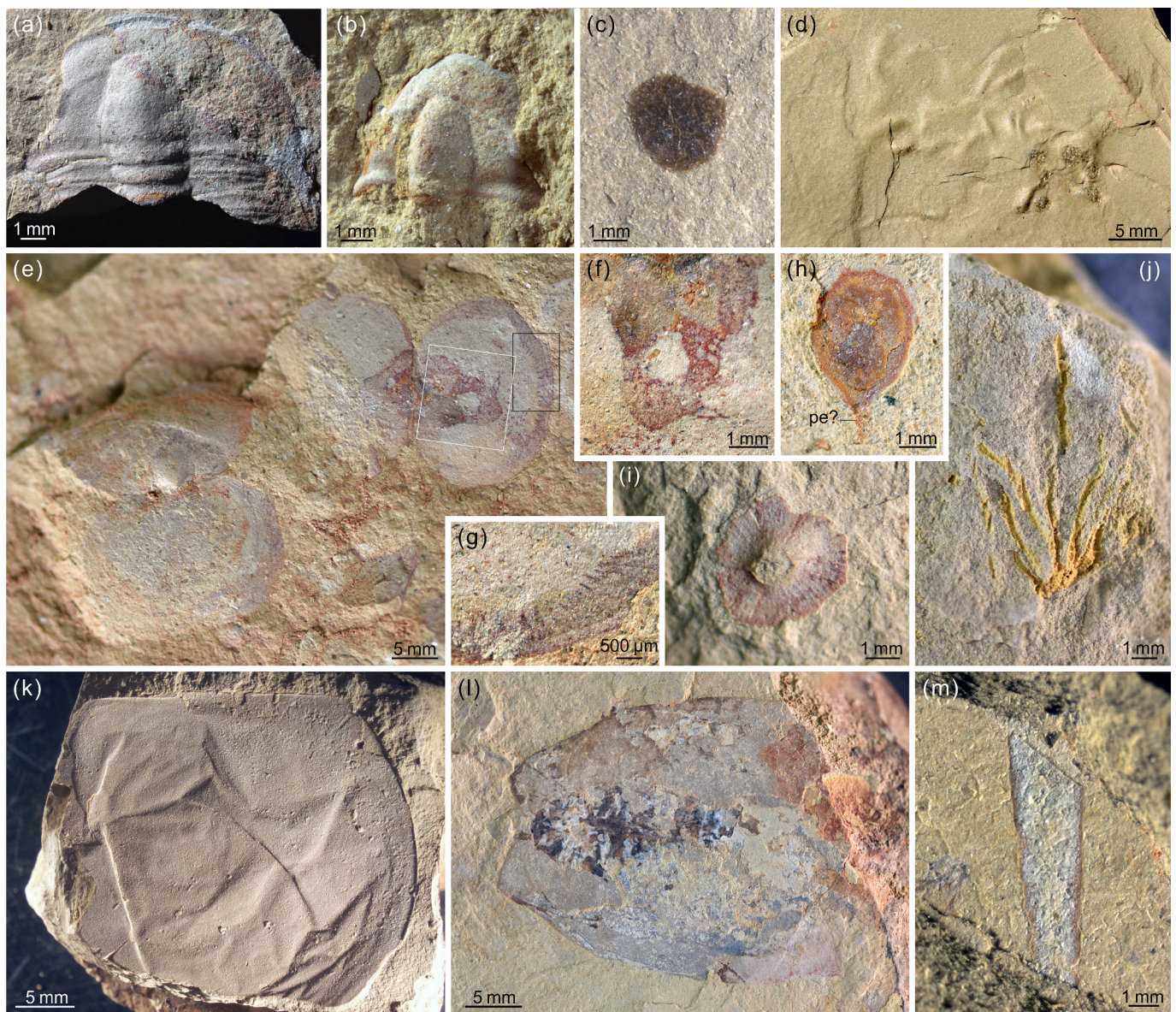

Fig. 2. Animals yielded from the *Wiwaxia*-bearing succession in Douposi Formation, Longzhaosi section. (**a**) Cephalon of trilobite *Kunmingaspis*, NIGP 203478. (**b**) Cephalon of trilobite *Chittidiella*, NIGP 203479. (**c**) Alga, NIGP 203480. (**d**) Trace fossils, NIGP 203481. (**e**) Articulated acrotretoid brachiopods with the right one preserved soft parts, NIGP 203482; white box indicates the position of (**f**) and black box indicates the location of (**g**). (**f**) Visceral organs. (**g**) Setae located at shell margin. (**h**) Pyritized linguloid brachiopod with a possibly illy preserved pedicle, NIGP 203483. (**i**) *Scenella*, NIGP 203484. (**j**) Arms of eocrinoid echinoderm, NIGP 203485. (**k**) An undetermined hymenocarine arthropod, NIGP 203486. (**l**) An unnamed ventulicoliid species with soft organs, NIGP 203487. (**m**) Tubular animal, NIGP 203488. Abbreviations: pe, pedicle.

microscope (Axio Zoom V16), and a field emission scanning electron microscope (FSSEM; instrument model TESCAN MAIA 3 GMU) equipped with energy dispersive X-ray spectroscopy (EDX). These analyses were carried out in the Experimental Technologies Center of NIGPAS. Specimen NIGP 203489 underwent additional examination using a micro-region X-ray fluorescence spectrometer (micro-XRF; instrument model Bruker M4 Plus Tornado) at Shanghai Boyue Instrument Co., LTD. Illustrations and photographs were produced and edited using Coreldraw 2018 and Adobe Photoshop 2020. Specimens were measured using ImageJ 1.47 V software, and statistical data were analyzed in Microsoft Excel (version 2403) and Origin 2018.

Palaeogeographic and stratigraphic distributions of *Wiwaxia* were derived from previously published works (Conway Morris, 1985; Zhao et al., 1994; Porter, 2004; Ivantsov et al., 2005a, 2005b; Fatka et al., 2011; Harvey and Butterfield, 2011; Zhao, 2011; Butterfield and Harvey, 2012; Harvey et al., 2012; Pedder, 2012; Palacios et al., 2014; Sun et al., 2014; Yang et al., 2014; Conway Morris et al., 2015; Zhang et al., 2015; Zhao et al., 2015; Smith et al., 2016; Slater et al., 2017).
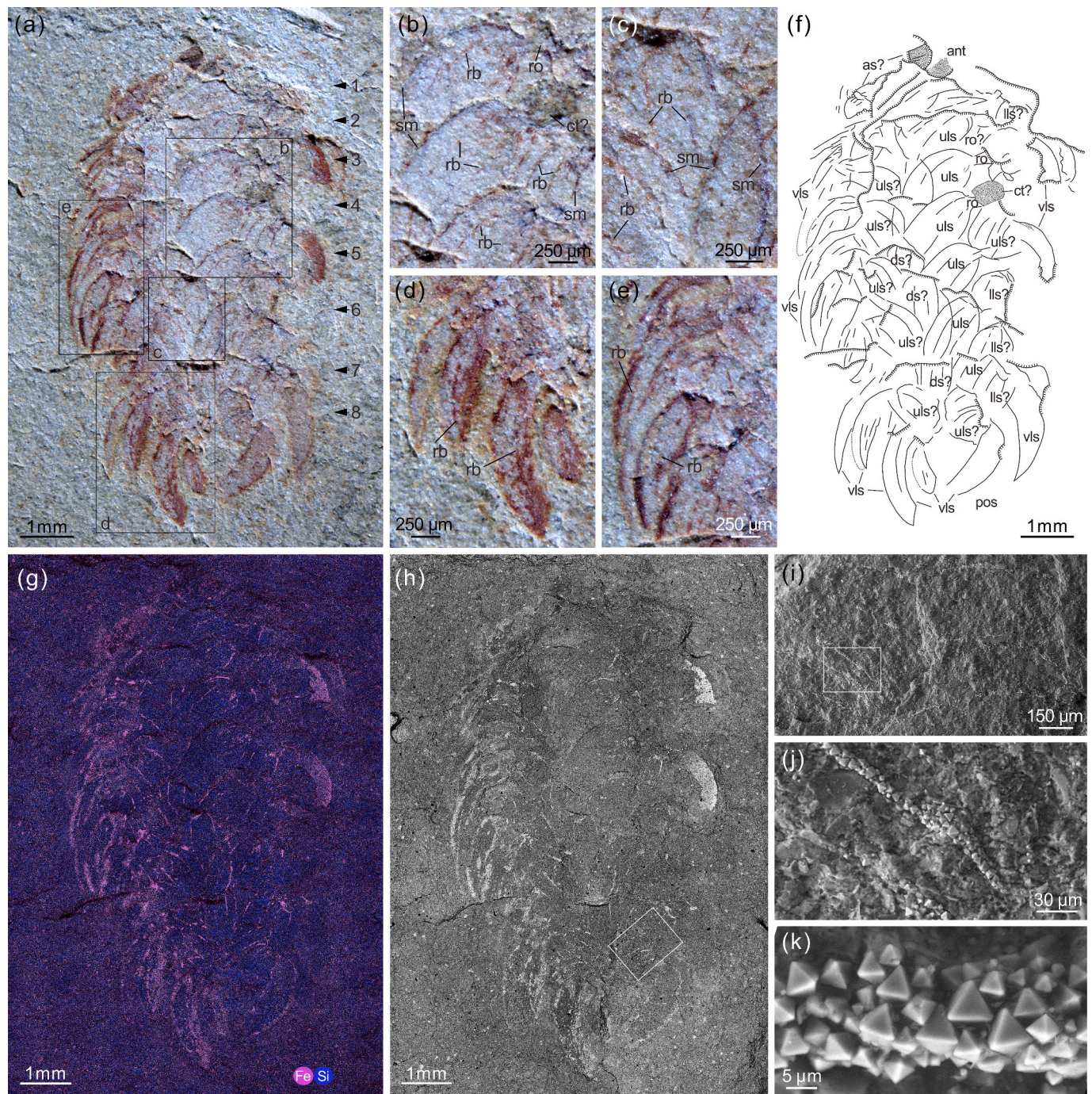

Fig. 3. *Wiwaxia douposiensis* sp. nov., articulated specimen from the Douposi Formation in Longzhaosi section, NIGP 203489. (**a**) Image captured under natural lighting; arrowheads indicate the inferred rows of transversely arranged sclerites; boxes denote the position of (**b-e**). (**b, c**) Magnification of the boxed area in (**a**) showing structures of upper-lateral sclerites. (**d, e**) Enlarged view of the boxed area in (**a**); ventral-lateral sclerites with ribs. (**f**) Interpretive illustration. (**g**) Enrichment of iron (Fe) observed by EDX. (**h**) Backscattered electron (BSE) image. (**i**) Close-up of the marked area in (**h**) showing ribs. (**j**) Enlarged view of the boxed area in (**i**); ribs are composed of octahedral pyrites. (**k**) Detail of octahedral pyrites. Abbreviations: ant, anterior; as, anterior sclerite; ct, connective tissue; ds, dorsal sclerite; lls, lower-lateral sclerite; pos, posterior; rb, rib; ro, root; sm, sclerite margin; uls, upper-lateral sclerite; vls, ventro-lateral sclerite.

The phylogenetic analysis data matrix consists of 10 taxa and 18 characters (Supplementary Data). Taxa or sclerites were selected based on clear and distinguishable characters. We generated topologies for weighted analyses, with inapplicable states treated as "missing" coding. A range of k values (1, 2, 4 and 10) were used to conduct implied-weight-based cladograms, and their results were identical or similar. Here, we only discussed the analyses using k = 2. Data set was run in

PAUP* v4.0a169 (Swofford, 1998), and tree construction was based on parsimony, treating all characters as unordered. Analysis was set to be root on *Wiwaxia foliosa* + *W. papilio* for their substantially earlier age than other taxa. A heuristic search was set using 10,000 additional sequence replicates with tree-bisection-reconnection (TBR) branch-swapping algorithm. A strict consensus tree was used to summarize the results of parsimony analyses. Cladograms were edited in FigTree
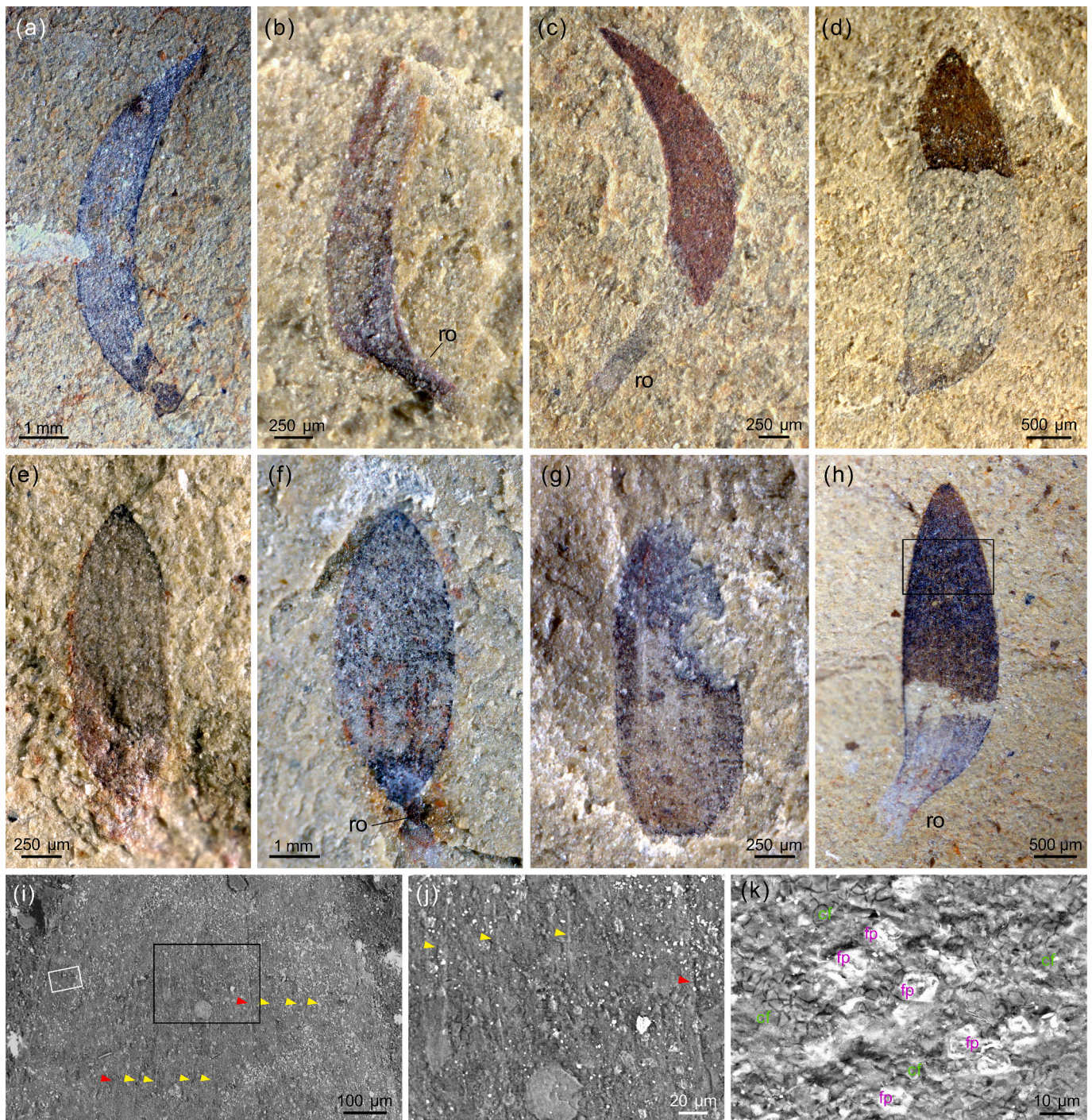

Fig. 4. Isolated sclerites of *Wiwaxia douposiensis* sp. nov. from the Douposi Formation in Longzhaosi section. (**a-d**) Ventro-lateral sclerites; NIGP 203490 for (**a**), NIGP 203491 for (**b**), NIGP 203492 for (**c**), Ventro-lateral sclerite, NIGP 203497 for (**d**). (**e, f**) Lower-lateral sclerites; NIGP 203494 for (**e**) and NIGP 203495 for (**f**). (**g**) Dorsal sclerite, NIGP 203496. (**h**) Ventro-lateral? sclerite NIGP 203493. (**i**) Enlarged view of boxed area in (**h**), exhibiting ribs; red arrowheads indicate thicker ribs and yellow arrowheads indicate finer ribs. (**j**) Details of the thicker (red arrowhead) and finer ribs (yellow arrowheads) in the black box of (**i**). (**k**) Close-up of the area in the white box in (**i**), showing cracked carbon film and oxidized framboid pyrites. Abbreviations: cf., carbon film; fp, framboid pyrite. (For interpretation of the references to colour in this figure legend, the reader is referred to the web version of this article.)

v1.4.4.

4. Systematic palaeontology

Family Wiwaxiidae Walcott, 1911
Genus *Wiwaxia* Walcott, 1911
Type species *Wiwaxia corrugata* (Matthew, 1899), Cambrian Wuliuan Burgess Shale Member, Stephen Formation, British Columbia, Canada.
Wiwaxia douposiensis sp. nov.

Etymology. Species name was derived from the stratigraphic interval where the fossils were discovered.

Holotype. NIGP 203489 (Fig. 3), an articulated specimen.

Paratype. NIGP 203493 (Fig. 4h-j), a two order rib-bearing sclerite.

Diagnosis. Complete individual is ovoid in dorsal view. Two-order of sclerite ribs: two prominent ribs interspersed with thin ribs on sclerites measuring 2–6 mm in length. The sclerites are relatively slender, and exhibit lower width to length ratios, with upper lateral sclerites appearing wider relative to body length, distinguishing them from other species (Fig. 5).

Stratigraphy and locality. Specimens were collected from the yellowish-green shales, siltstones, and fine-grained sandstones of the Douposi Formation at the Longzhaosi section, belonging to the *Kunmingaspis – Chittidilla* Zone (Cambrian Stage 4), Yiliang County, Kunming City, Yunnan Province, China.

Description. The singular articulated specimen preserved in dorsal view, exhibits an ovoid shape (Fig. 3a, f, g, h). This individual measures around 7.2 mm in length and is adorned with imbricated sclerites, likely arranged in eight transverse rows (Fig. 3a). No spines are observed. The most distinct elements are the ventro-lateral sclerites, which are closely spaced, and inclined posteriorly (Fig. 3a, d, e). Well-preserved ones exhibit sickle-shaped characteristics near the posterior end (Fig. 3a, d), with the remains displaying moderate preservation (Fig. 3a, e). Some of the ventro-lateral sclerites preserved ribs (Fig. 3d, e). One series of upper-lateral sclerites preserved with a total of six recognizable (Fig. 3a, f), and the upper four preserved two prominent ribs (Fig. 3b, c), potentially their roots, with one possibly preserving a connective tissue (Fig. 3b). These partially buried sclerites are symmetrical, featuring two major ribs and pointing backward at an angle of ca. 46° from the central axis of the body. Other sclerites covering the dorsal and lateral regions are challenging to identify due to superposition and taphonomic bias, with some of their margins difficult to distinguish from ribs. Nonetheless, several sclerites can be inferred by their positions and rib directions (Fig. 3f).

In addition to the articulated specimen, 13 isolated sclerites were also found. The ventro-lateral sclerites are asymmetrical, and some are cultrate (Figs. 4a-c, 5; length = 3.04–7.69 mm, width = 0.56–2.45 mm, length/width = 5.4–6.5), bearing a stout root with a broad base (Fig. 4b; 0.43 mm long, maximum basal width is 0.27 mm) or bearing a long and
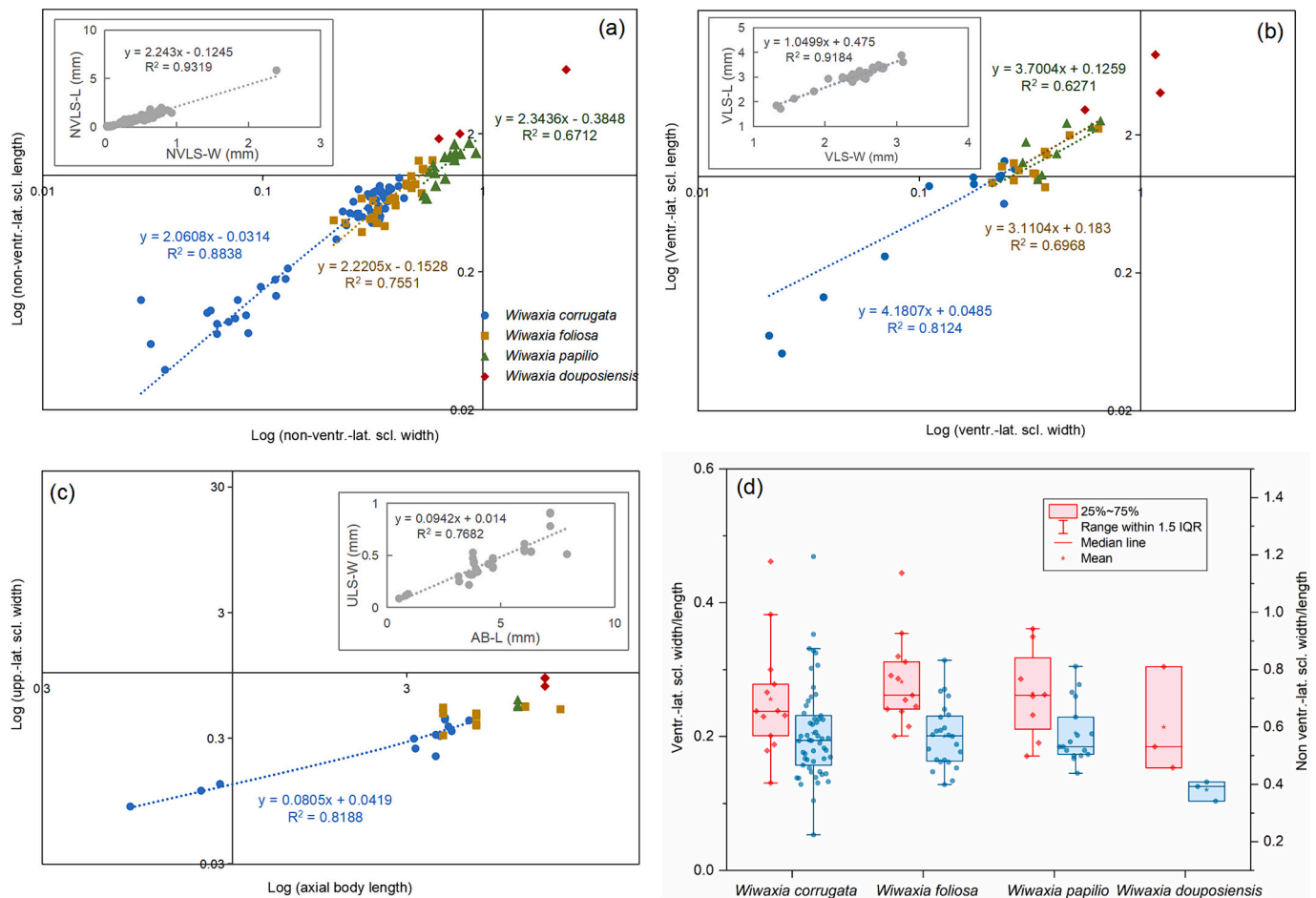

Fig. 5. Bivariate and box plots of sclerites measurements in *Wiwaxia* species. (**a**) Logarithmic plots of non-ventro-lateral sclerites' width to their length; diagram in the upper-left corner shows nonlogarithmic plots of the same data. (**b**) Logarithmic plots of ventro-lateral sclerites' width to their length; chart in the upper-left corner shows nonlogarithmic plots of the same data. (**c**) Logarithmic plots of axial body length to upper-lateral sclerite width; graph in the upper-right corner shows nonlogarithmic plots of the same data. (**d**) Box plots of the width to length ratios of the ventro-lateral and non-ventro-lateral sclerites. Measurements of *W. papilio*, *W. foliosa* and *W. corrugata* from Zhang et al. (2015). Abbreviations: NVLS-L, length of non-ventro-lateral sclerite; NVLS-W, width of non-ventro-lateral sclerite; VLS-L, length of ventro-lateral sclerite; VLS—W, width of ventro-lateral sclerite.

slender tubular root (Fig. 4c; length = 0.4 mm, width = 0.1 mm), whereas some are more rounded (e.g. Fig. 4d; length = 4.04 mm, width = 1.23 mm, length/width = 3.28). Two lower-lateral sclerites are oval with pointed tips (Fig. 4e, f), measuring around 1.85 and 5.85 mm in length, and 0.63 and 2.39 mm in width, resulting in length/width ratios of 2.9 and 2.4; one of them experienced slight post-mortem deformation due to lateral compression (Fig. 4e); another one preserved two incomplete major ribs and a partial root (Fig. 4f). One sclerite, measuring 3.42 mm long and 1.13 mm wide (length/width = 3.01), displays a transitional morphology of an asymmetrical ventro-lateral sclerite and a symmetrical lower-lateral sclerite (Fig. 4h); its tubular root is 0.68 mm long, 0.43 mm wide, and slightly expanded at the base; the sclerite surface is covered by faint longitudinal ribs, with a count can reach over 10 (Fig. 4i, j, rib interval 40–97 μm); although the thick and thin ribs may not be easily distinguishable on this specimen, considering the presence of two prominent ribs in some other sclerites (e.g. Figs. 3a-c and 4f), *Wiwaxia* in this study likely bears a two-order rib pattern. A single dorsal sclerite is available but lacks a preserved root (Fig. 4g). This specimen is slightly asymmetrical and reaches its maximum width at the lower-middle part (length = 2 mm, maximum width = 0.79 mm, length/width = 2.5).

Remarks. Wiwaxia douposiensis resembles *W. papilio* (Zhang et al., 2015), *W. foliosa* (Yang et al., 2014) and juveniles of *W. corrugata* (Smith, 2014), in terms of absence of spines, body shape, and sclerite general outline and distribution (Figs. 3, 5). However, the new materials also exhibit differences with the above three species in: (1) having lower sclerite width/length ratios (Fig. 5a, b, d); (2) possessing slightly wider upper-lateral sclerites relative to axial body length (Fig. 5c). In terms of longitudinal striations, *W. douposiensis* exhibits two-order ribs. However, the thin ribs, although present, are less frequently preserved and more challenging to observe compared to their prominent counterparts. The fainter ribs are only discernible on one isolated sclerite (Fig. 4h). The same rib pattern also occurs in *W. corrugata* (Butterfield, 1990, fig. 3a, b and d; Harvey et al., 2012; Zhao et al., 1994, and on sclerites from Monastery Creek Formation (Porter, 2004, fig. 11.7), Earlie Formation (Butterfield and Harvey, 2012, fig. 1H) as well as Mount Cap Formation (Harvey and Butterfield, 2011, fig. 7a; Butterfield and Harvey, 2012, fig. 1A); although, rib number and interval vary. In contrast, sclerites of *W. papilio*, *W. foliosa* and that from Monastery Creek Formation have a single order of ribs (Porter, 2004, fig. 11.8, 11.11; Yang et al., 2014; Zhang et al., 2015). However, the presence of a single-order rib pattern could be due to a taphonomic artifact where thin ribs are barely preserved, a phenomenon observed in most specimens in this study, or it may reflect a situation similar to that seen in *W. corrugata*. In *W. corrugata*, the appearance of "two-order" and "one order" morphologies depends on whether one is examining small fossils films (SCFs) or larger macrofossils preserved within bedding planes (Butterfield, 1990; Butterfield and Harvey, 2012; Smith, 2014). For lack of evidence to support above notion, we rely on the original descriptions of *W. papilio* and *W. foliosa* (Yang et al., 2014; Zhang et al., 2015). The shortage of comparative specimens of *W. douposiensis* hampered detailed comparison with other species.

5. Preservation

The presence of the articulated *Wiwaxia douposiensis* suggests rapid burial, either while alive or shortly after death. Alternatively, their sclerites may readily detach following mild oxidation, akin to the characteristics observed in polychaete annelids (Butterfield, 1990). Substantial decomposition of the organism occurs post-burial; otherwise, maintaining the complete articulated individual intact would be challenging. Isolated sclerites are found scattered on bedding planes, suggesting that either they were shed scales, or the organisms underwent significant decay before burial, possibly experiencing transportation and/or current disturbance. *Wiwaxia* specimens are preserved through carbonaceous films and/or pyritization subsequently replaced

by iron oxides (Figs. 3, 4), which are typical taphonomic pathways in Burgess Shale-type lagerstätten, especially in the Chengjiang biota (e.g. Gabbott et al., 2004; Zhu et al., 2005; Butterfield et al., 2007; Gaines et al., 2008, 2012).

Various pyrite textures reflect variations in the environmental conditions within the porewaters (Grimes et al., 2002), and pyrite oxidation has little effect on redox assessment (Chang et al., 2020). Preservation of isolated sclerites is characterized by both carbonaceous films and framboidal pyrites (Fig. 4a-h, k). The diameter of these framboidal pyrites ranges from 6.1 μm to 11.4 μm ($n = 32$, average = 8.8 μm, standard deviation = 1.33, coefficient of skew = 0.24), and individuals over 10 μm constitute around 22%, suggesting a dysoxic microenvironment based on various criteria concerning the redox conditions and their corresponding features of pyrite framboids (Wilkin et al., 1996; Bond and Wignall, 2010; Wei et al., 2016; Chang et al., 2020). The rapid decay of sclerites might have served as favorable substrates fostering the activity of sulfate-reducing bacteria, leading to the generation of hydrogen sulfide (H_2S) from sulfate in seawater and the formation of pyrite nuclei (Briggs et al., 1996; Gabbott et al., 2004). Additionally, elevated iron concentrations in pore-water solutions and minimal organic content in the sediment likely enabled the production of framboidal pyrites restricted on animal tissues (Briggs et al., 1996; Gabbott et al., 2004). Furthermore, the euhedral outline without microcrystals (Fig. 4k) suggests that these framboidal pyrites experienced recrystallization and evolved into the final stage during later diagenesis (Merinero et al., 2008).

The articulated *Wiwaxia* has a high concentration of iron, which is especially enriched in sclerite margins and the area near the roots (Fig. 3g). The ribs and margins of sclerites are outlined by densely arranged oxidized octahedral pyrites (Fig. 3i-k). These minerals have a wide range of grain sizes, varying from 0.9 μm to 10. 3 μm with an average of 5 μm ($n = 105$). The alignment, euhedral morphology, and absence of framboidal pyrites indicate an ideal condition for diffusion of $FeS_{(aq)}$ complex (Gabbott et al., 2004), e.g. low concentration of H_2S, longer crystallization time, and more reduced eH (Grimes et al., 2002; Gabbott et al., 2004). During subsequent diagenesis, euhedral pyrites were oxidized within oxic porewaters.

6. Discussion

6.1. Geological and ecological distributions of Wiwaxia

This research enhances our temporal and spatial understanding of *Wiwaxia*. Since *Wiwaxia*'s first identification in the middle Cambrian Burgess Shale biota (Walcott, 1911), it has been documented on seven paleocontinents and in 22 deposits spanning from Cambrian Series 2 Stage 3 to Miaolingian Guzhangian (Figs. 6, 7). While wiwaxiid-like sclerites have been described from the Ordovician (Kimmig et al., 2019), potentially extending the distribution of *Wiwaxia*, their precise affinity awaits further evaluation. Hitherto, Laurentia boasts the most occurrences of *Wiwaxia*, ranging from Cambrian Stage 4 to Guzhangian (Fig. 6), with fossil records primarily from Canadian deposits (Conway Morris, 1985; Butterfield, 1994; Harvey and Butterfield, 2011; Butterfield and Harvey, 2012; Smith, 2014). Meanwhile, the Nolichucky Shale in the USA yields the youngest record of this taxon (Pedder, 2012). South China holds the second-highest number of fossil occurrences and records the earliest known appearance of *Wiwaxia* in the Cambrian Stage 3 Chengjiang Lagerstätte (Fig. 6; Zhang et al., 2015; Zhao et al., 2015). Other reports are scattered across NW Gondwana (Fatka et al., 2011; Palacios et al., 2014), Baltica (Slater et al., 2017), Siberia (Ivantsov et al., 2005a, 2005b), Australia (Porter, 2004), and South America (Smith et al., 2016). Among these records, small carbonaceous fossils are the most common forms, constituting over 50%, followed by around 44% of fossils compressed in shales that yield Burgess Shale-type biotas. Phosphatic casts of *Wiwaxia* sclerites are relatively rare (Fig. 6).

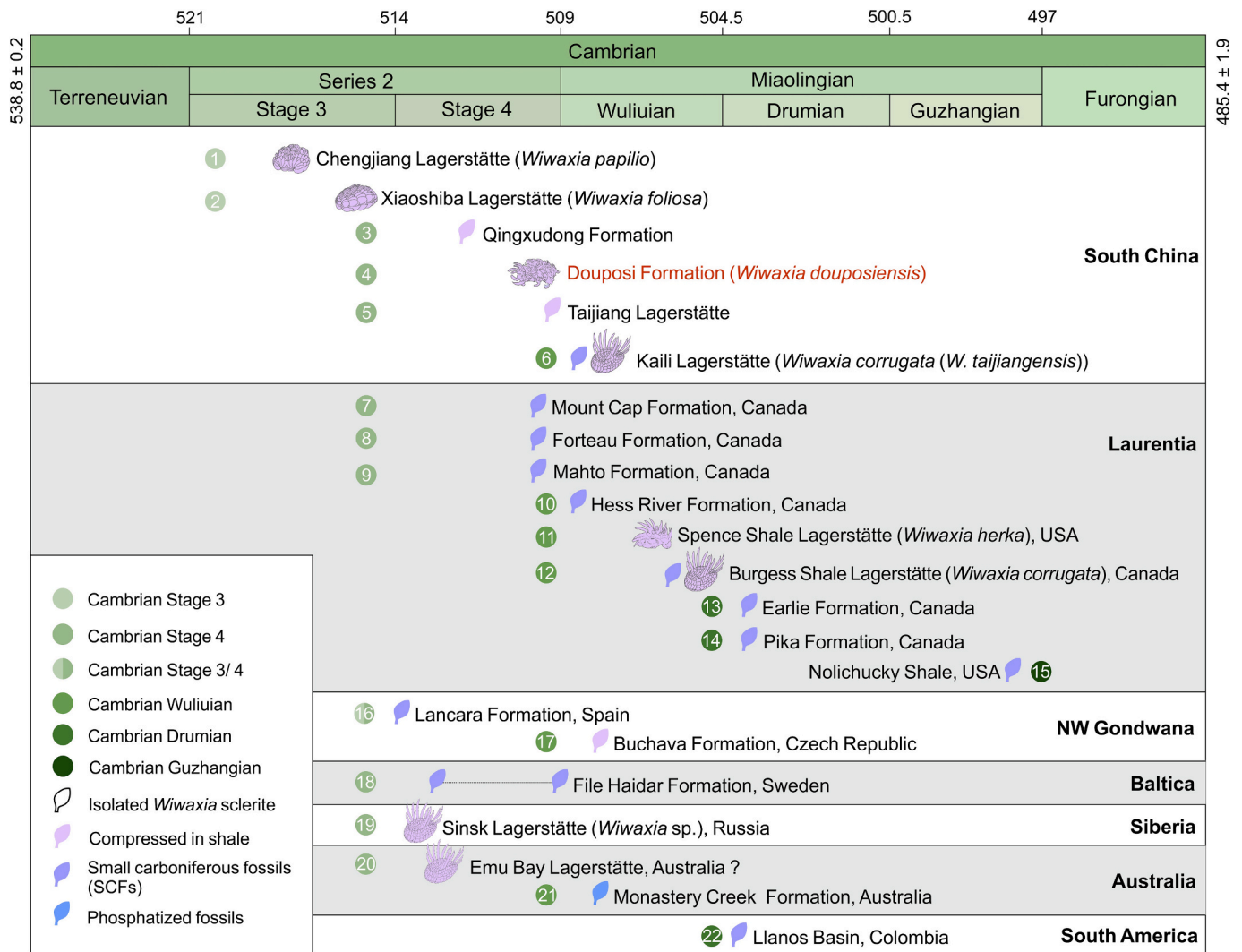The origin of *Wiwaxia* remains a mystery. Molecular clock analysis

Fig. 6. Stratigraphic distribution of *Wiwaxia*.

indicates that lophotrochozoans diverged in the early Ediacaran (Erwin et al., 2011; dos Reis et al., 2015). However, unequivocal fossil record shows a Cambrian origin of most lophotrochozoan lineages (Kouchinsky et al., 2012; Budd and Jackson, 2016). Halkieriids, another challenging lophotrochozoan group characterized by multi-plated scleritomes with biomineralization, were grouped with wiwaxiids to form a novel category—halwaxiid (Conway Morris and Caron, 2007). However, this proposition has faced challenges in subsequent works (Zhao et al., 2017). Halkieriid sclerites are pervasive in the early Cambrian small shelly fossils (He et al., 2023 and references therein). In contrast, *Wiwaxia* sclerites are notably absent in both Ediacaran and Cambrian Terreneuvian fossil assemblages (Slater et al., 2017; Slater and Bohlin, 2022). If the absence observed is not attributable to sampling or taphonomic bias, it is highly probable that *Wiwaxia* had not yet evolved during that period. In this case, it can be inferred that the *Wiwaxia* body plan originated during the Cambrian Age 3. Currently, there have been no reported deposits of *Wiwaxia* outside of South China from the same time period. Despite the presence of the Sirius Passet Lagerstätte in North Greenland, which is a Burgess Shale-type fauna from the Cambrian Age 3 and situated in an outer shelf environment (Harper et al., 2019), no *Wiwaxia* has been discovered since 1984 (Conway Morris et al., 1987; Harper et al., 2019). Moreover, *Wiwaxia* is absent in the deep-water deposits of Cambrian Stage 3 in South China, such as the Niutitang, Hetang and Huangboling Formations, which are located in slope environments and contain sponge faunas (Wu et al., 2005; Xiao

et al., 2005; Yang et al., 2005). Although sampling bias cannot be definitively ruled out, based on the presently known assemblages (Figs. 6, 7), a tentative biogeographical pattern is proposed. These animals might have originated in the shallow-water of South China under a humid warm climate (Figs. 6, 7; Zhang et al., 2015; Zhao et al., 2015). In addition to thriving endemically, *Wiwaxia* began to spread to nearby plates from the end of Cambrian Age 3, i.e. Gondwana, Siberia, Australia, and Baltica (Figs. 6, 7). Simultaneously, they expanded into and occupied deep-water ecospaces, e.g. the Qingxudong (=Tsinghsutung) Formation (Sun et al., 2014) and the Sinsk biota (Ivantsov et al., 2005b). Since the middle-late Cambrian Age 4, *Wiwaxia* had rapidly spread in Laurentia (Figs. 6, 7). The Cambrian Stage 4 witnessed the peak of population dispersal and migration of this genus (Fig. 6). During early Drumian, some individuals already thrived in high-latitude, dry and cold regions (Smith et al., 2016). The worldwide distribution and strong environmental adaptability suggest epi-benthic *Wiwaxia* had planktonic larvae, able to survive in a wide range of ecological constraints.

Despite *Wiwaxia* being common in the fossil record, articulated individuals are scarce and only yielded from seven localities, including South China Chengjiang, Xiaoshiba, Douposi, Kaili Lagerstätten, Laurentia Spence Shale and Burgess Shale Lagerstätten, and Siberia Sinsk Lagerstätte (Figs. 6, 7). The Australia Emu Bay Shale potentially harbors another presence of articulated *Wiwaxia* (Porter, 2004, p.588); however, as of now, no formal publication on this finding is available. Among
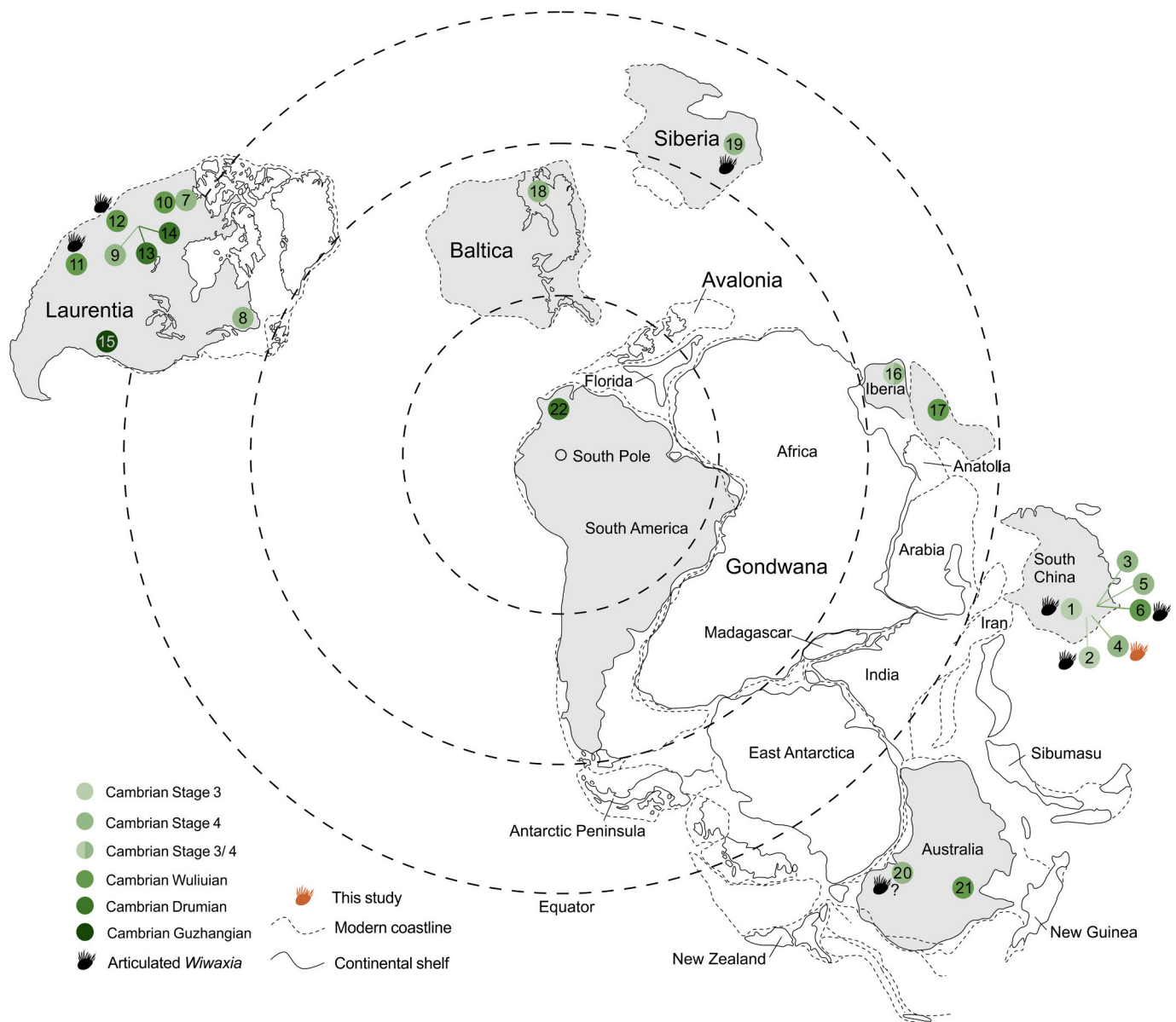
Fig. 7. Paleogeographic distribution of *Wiwaxia* (adapted from Slater et al., 2017). Further details on occurrence data refer to Fig. 6.

these articulated fossils, individuals from shallow-water settings (Chengjiang, Xiaoshiba and Douposi) are under 9 mm and lack spines (Yang et al., 2014; Zhang et al., 2015), comparable to those of *W. corrugata* juveniles (Smith, 2014). In contrast, it is easier to find articulated individuals belonging to *Wiwaxia* adults from deep-water settings, e.g. Kaili, Spence Shale and Burgess Shale biotas (Conway Morris, 1985; Smith, 2014; Sun et al., 2014; Conway Morris et al., 2015). The absence of larger articulated specimens in these shallow waters was suggested to result from taphonomic bias, as larger individuals with low density are easier to be transported or disarticulated (Yang et al., 2014), or from a failure to reach maturity through migration or predation pressure on adults (Zhang et al., 2015). However, isolated sclerites from the Douposi Formation (Fig. 4c), Chengjiang fauna (Zhao et al., 2015) and File Haidar Formation (Slater et al., 2017) indicate the presence of adults. Therefore, the lack of complete adults in shallow waters is more likely a taphonomic artifact relating to specific preservational conditions. Alternatively, early originated species are neotenic, and dorsal spines are a derived character, but this assumption needs more material to verify.

6.2. Morphological diversity of Wiwaxia

Evaluating the morphological diversity of *Wiwaxia* is challenging due to sampling biases and the predominance of isolated sclerites in the fossil record. Nevertheless, existing data can still reveal some measurable morphologies based on detailed sclerite characteristics, providing a certain level of reference value (Figs. 5, 8). Articulated specimens indicate that the general body plan of *Wiwaxia* is relatively conserved, characterized by body shape, differentiation of distinct zones, and the arrangement of sclerites in rows (Yang et al., 2014). Moreover, in measurable species (Fig. 5), robust linear correlations exist between non-ventro-lateral sclerite width and length ($R^2 = 0.9319$), ventro-lateral sclerite width and length ($R^2 = 0.9184$), as well as axial body length and upper-lateral sclerite width ($R^2 = 0.7682$).

Beyond these common features, various diagnostic characteristics of sclerites have been described, including the number of transverse rows, aspect ratios, ornamentation of pits or tubercles, ribbing number and pattern, and distal collars (Butterfield, 1990; Porter, 2004; Butterfield and Harvey, 2012; Harvey et al., 2012; Smith, 2014; Yang et al., 2014; Zhang et al., 2015). However, their roles in evaluating diversity and
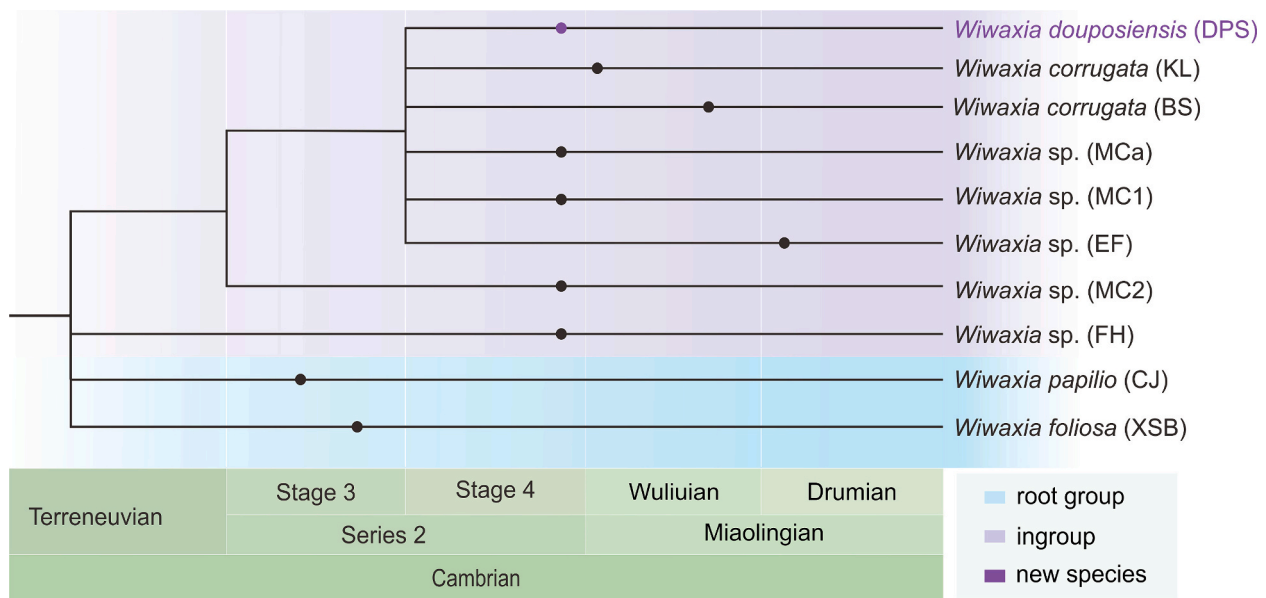
Fig. 8. Strict consensus of 516 parsimony trees using implied weighting with k = 2; best tree: CI (Consistency Index) = 0.75, RI (Retention Index) = 0.643, RC (Rescaled Consistency Index) = 0.482, Goloboff fit = −6.75. Filled circles denote the age of taxa. Abbreviations: BS, Burgess Shale biota; CJ, Chengjiang biota; DPS, Douposi Formation; EF, Earlie Formation; FH, File Haidar Formation; MC, Monastery Creek Formation; MC1, sclerite with tubercles (Porter, 2004, fig. 11.7, 11.9, 11.10); MC2, sclerite with pits (Porter, 2004, fig. 11.8, 11.11); MCa, Mount Cap Formation.

differentiating clades within *Wiwaxia* remain uncertain. To address this, we produced a cladogram using parsimony analysis based on current knowledge (Fig. 8). *W. papilio* and *W. foliosa*, which originated during the Cambrian Age 3, were designated as the root group, distinguishing by their single-order ribs devoid of sclerite ornamentation. *W.* sp. (FH), bearing a distal collar without ornamentation, cannot be distinguished from these two species. *W.* sp. (MC2) is characterized by single-order ribs and pits on sclerites, bridging taxa with single-order ribs devoid of ornamentation and those with a two-order rib pattern and tubercle ornamentation. *W. douposiensis* is grouped with *W. corrugata* (KL, BS) by their two-order ribs, likely evolved as an adaptation to enhance scale thickness and reinforcement. The number of transverse rows of sclerites and aspect ratios of non-ventro-lateral sclerites also contribute to the classification of these three taxa. Other isolated sclerites of MCa, MC1 and EF cannot be distinguished from them.

The results indicate that rib pattern, ornamentation (pits or tubercles), aspect ratio, and the number of transverse rows of sclerites are informative characters in cladistic taxonomy, whereas the role of the distal collar appears less significant. The significance of spine characteristics remains unexplored in this study, necessitating further evaluation.

In summary, *Wiwaxia* exhibits a degree of phenotypic variability. However, it is evident that the current analysis is far from exhaustive, and the resolution is low (Fig. 8). Enhancing the precision of *Wiwaxia* taxonomy, diversity, and phylogenetic analyses heavily depends on the availability of better-preserved materials. It is challenging but crucial to determine whether character variations are ontogenetic, intraspecific, or interspecific differences in future work. Investigating the mechanisms underpinning morphological variation, such as ecological plasticity and convergence, also remains a significant research interest.

7. Conclusions

(1) The new species *Wiwaxia douposiensis* from the Cambrian Stage 4 Douposi Formation includes an articulated specimen (<8 mm long, without spine) and 13 isolated sclerites. The examined sclerites exhibit a distinctive two-order rib pattern and larger length/width ratios compared to other measurable existing species.

(2) Preservation of specimens involves carbonaceous film and pyritization. The articulated specimen, featuring densely arranged oxidized octahedral pyrites, suggests a rapid burial in a microenvironment with a low concentration of H_2S, longer crystallization time, and more reduced eH. Isolated sclerites, interpreted as shed scales or the result of significant decay prior to burial, exhibit characteristics of oxidized framboidal pyrites, indicating entombment in a dysoxic microenvironment.

(3) Discovery of *Wiwaxia douposiensis* enriches our understanding of the spatial and temporal distributions of these animals. If not influenced by sampling and taphonomic bias, the appearance of *Wiwaxia* no earlier than the Cambrian Age 3 suggests that these animals diversified during the peak of the Cambrian Explosion. They likely originated in shallow water under humid and warm conditions in South China before spreading to other continents, and adapting to various environments, including deep-water settings, and dry and cold climates, with a dispersal peak during Cambrian Age 4.

(4) Statistical analysis reveals that *Wiwaxia* maintains a conservative body plan and consistent sclerite aspect ratios. However, individual species exhibit diversity in sclerite characteristics. Despite the low resolution, cladogram analysis suggests a degree of morphological plasticity within *Wiwaxia*. Rib patterns, sclerite aspect ratios, ornamentation, and the number of sclerite rows are informative features for cladistic taxonomy. To enhance the precision of classification, diversity assessment, and phylogenetic analysis of *Wiwaxia*, better-preserved materials are essential.

CRediT authorship contribution statement

Haijing Sun: Writing – review & editing, Writing – original draft, Visualization, Validation, Software, Methodology, Investigation, Formal analysis, Data curation, Conceptualization. **Fangchen Zhao:** Writing –

review & editing, Visualization, Resources, Project administration, Investigation, Funding acquisition, Conceptualization. **Ruolin Wu:** Writing – review & editing, Visualization, Software, Formal analysis. **Han Zeng:** Writing – review & editing, Methodology. **Zhixin Sun:** Writing – review & editing, Investigation.

Declaration of competing interest

The authors declare that they have no known competing financial interests or personal relationships that could have appeared to influence the work reported in this paper.

Data availability

All data generated or analyzed during this study are included in this article and its supplementary information files.

Appendix A. Supplementary data

Supplementary data to this article can be found online at https://doi. org/10.1016/j.gloplacha.2024.104507.

References

Bengtson, S., Conway Morris, S., 1984. A comparative study of lower Cambrian *Halkieria* and middle Cambrian *Wiwaxia*. Lethaia 17, 307–329. https://doi.org/10.1111/j.1502-3931.1984.tb02022.x.

Bond, D.P.G., Wignall, P.B., 2010. Pyrite framboid study of marine Permian–Triassic boundary sections: A complex anoxic event and its relationship to contemporaneous mass extinction. Geol. Soc. Am. Bull. 122, 1265–1279. https://doi.org/10.1130/b30042.1.

Briggs, D.E.G., Raiswell, R., Bottrell, S.H., Hatfield, D., Bartels, C., 1996. Controls on the pyritization of exceptionally preserved fossils: an analysis of the lower Devonian Hunsrqck Slate of Germany. Am. J. Sci. 296, 633–663. https://doi.org/10.2475/ajs.296.6.633.

Budd, G.E., Jackson, I.S.C., 2016. Ecological innovations in the Cambrian and the origins of the crown group phyla. Philos. Trans. R. Soc. B 371, 20150287. https://doi.org/10.1098/rstb.2015.0287.

Butterfield, N.J., 1990. A reassessment of the enigmatic Burgess Shale fossil *Wiwaxia corrugata* (Matthew) and its relationship to the polychaete *Canadia spinosa* Walcott. Paleobiology 16, 287–303. https://doi.org/10.1017/s0094837300010009.

Butterfield, N.J., 1994. Burgess Shale-type fossils from a Lower Cambrian shallow-shelf sequence in northwestern Canada. Nature 369, 477–479. https://doi.org/10.1038/369477a0.

Butterfield, N.J., 2006. Hooking some stem-group "worms": fossil lophotrochozoans in the Burgess Shale. BioEssays 28, 1161–1166. https://doi.org/10.1002/bies.20507.

Butterfield, N.J., Harvey, T.H.P., 2012. Small carbonaceous fossils (SCFs): a new measure of early Paleozoic paleobiology. Geology 40, 71–74. https://doi.org/10.1130/g32580.1.

Butterfield, N.J., Balthasar, U.W.E., Wilson, L.A., 2007. Fossil diagenesis in the Burgess Shale. Palaeontology 50, 537–543. https://doi.org/10.1111/j.1475-4983.2007.00656.x.

Caron, J.B., Scheltema, A., Schander, C., Rudkin, D., 2006. A soft-bodied mollusc with radula from the Middle Cambrian Burgess Shale. Nature 442, 159–163. https://doi.org/10.1038/nature04894.

Chang, X.L., Huang, Y.G., Chen, Z.Q., Hou, M.C., 2020. The microscopic analysis of pyrite framboids and application in paleo•oceanography. Acta Sedimentol. Sin. 38, 150–165. https://doi.org/10.14027/j.issn.1000•0550.2019.099.

Conway Morris, S., 1985. The Middle Cambrian metazoan *Wiwaxia corrugata* (Matthew) from the Burgess Shale and *Ogygopsis* Shale, British Columbia, Canada. Philos. Trans. Royal Soc. B: Biol. Sci. 307, 507–582. https://doi.org/10.1098/rstb.1985.0005.

Conway Morris, S., Caron, J.-B., 2007. Halwaxiids and the early evolution of the lophotrochozoans. Science 315, 1255–1258. https://doi.org/10.1126/science.1137187.

Conway Morris, S., Peel, J.S., Higgins, A.K., Soper, N.J., Davis, N.C., 1987. A Burgess shale-like fauna from the lower Cambrian of North Greenland. Nature 326, 181–183. https://doi.org/10.1038/326181a0.

Conway Morris, S., Selden, P.A., Gunther, G., Jamison, P.G., Robiso, R.A., 2015. New records of Burgess Shale-type taxa from the middle Cambrian of Utah. J. Paleontol. 89, 411–423. https://doi.org/10.1017/jpa.2015.26.

dos Reis, M., Thawornwattana, Y., Angelis, K., Telford, M.J., Donoghue, P.C., Yang, Z., 2015. Uncertainty in the timing of origin of animals and the limits of precision in molecular timescales. Curr. Biol. 25, 2939–2950. https://doi.org/10.1016/j.cub.2015.09.066.

Erwin, D.H., Laflamme, M., Tweedt, S.M., Sperling, E.A., Pisani, D., Peterson, K.J., 2011. The Cambrian conundrum: early divergence and later ecological success in the early history of animals. Science 334, 1091–1097. https://doi.org/10.1126/science.1206375.

Fatka, O., Kraft, P., Szabad, M., 2011. Shallow-water occurrence of *Wiwaxia* in the Middle Cambrian of the Barrandian Area, Czech Republic. Acta Palaeontol. Pol. 56, 871–875. https://doi.org/10.4202/app.2009.0052.

Gabbott, S.E., Hou, X.G., Norry, M.J., Siveter, D.J., 2004. Preservation of Early Cambrian animals of the Chengjiang biota. Geology 32, 901–904. https://doi.org/10.1130/g20640.1.

Gaines, R.R., Briggs, D.E.G., Zhao, Y., 2008. Cambrian Burgess Shale–type deposits share a common mode of fossilization. Geology 36, 755–758. https://doi.org/10.1130/g24961a.1.

Gaines, R.R., Hammarlund, E.U., Hou, X., Qi, C., Gabbott, S.E., Zhao, Y., Peng, J., Canfield, D.E., 2012. Mechanism for Burgess Shale-type preservation. PNAS 109, 5180–5184. https://doi.org/10.1073/pnas.1111784109.

Grimes, S.T., Davies, K.L., Butler, I.B., Brock, F., Edwards, D., Rickard, D., Briggs, D.E.G., Parkes, R.J., 2002. Fossil plants from the Eocene London Clay: the use of pyrite textures to determine the mechanism of pyritization. J. Geol. Soc. Lond. 159, 493–501. https://doi.org/10.1144/0016-764901-176.

Harper, D.A.T., Hammarlund, E.U., Topper, T.P., Nielsen, A.T., Rasmussen, J.A., Park, T.-Y.S., Smith, M.P., 2019. The Sirius Passet Lagerstätte of North Greenland: a remote window on the Cambrian Explosion. J. Geol. Soc. Lond. 176, 1023–1037. https://doi.org/10.1144/jgs2019-043.

Harvey, T.H.P., Butterfield, N.J., 2011. Great Canadian *Lagerstätten* 2. Macro- and microfossils of the Mount Cap Formation (early and Middle Cambrian, Northwest Territories). Geosci. Can. 38, 165–173. https://journals.lib.unb.ca/index.php/GC/article/download/18965/20774?inline=1.

Harvey, T.H.P., Ortega-Hernández, J., Lin, J.-P., Zhao, Y.L., Butterfield, N.J., 2012. Burgess Shale-type microfossils from the middle Cambrian Kaili Formation, Guizhou Province, China. Acta Palaeontol. Pol. 57, 423–436. https://doi.org/10.4202/app.2011.0028.

He, Y.J., Pang, Y.C., Zhang, M.S., Hu, Q., Liang, S.Y., Lin, L., 2023. Phylogeny and taxonomy of *Halkieria*: progress and prospects. Acta Palaeontol. Sin. 62, 147–168. https://doi.org/10.19800/j.cnki.aps.2021073.

Ivantsov, A.Y., Krassilov, V.A., Leguta, A.V., Melnikova, L.M., Urbanek, A., Ushatinskaya, G.T., Malakhovskaya, Y.E., 2005a. Unique Sinsk localities of early Cambrian organisms. Trans. Palaeontol. Inst. 284, 1–143.

Ivantsov, A.Y., Zhuravlev, A.Y., Leguta, A.V., Krassilov, V.A., Melnikova, L.M., Ushatinskaya, G.T., 2005b. Palaeoecology of the Early Cambrian Sinsk biota from the Siberian Platform. Palaeogeogr. Palaeoclimatol. Palaeoecol. 220, 69–88. https://doi.org/10.1016/j.palaeo.2004.01.022.

Kimmig, J., Couto, H., Leibach, W.W., Lieberman, B.S., 2019. Soft-bodied fossils from the upper Valongo Formation (Middle Ordovician: Dapingian-Darriwilian) of northern Portugal. Sci. Nat. 106, 27. https://doi.org/10.1007/s00114-019-1623-z.

Kouchinsky, A., Bengtson, S., Runnegar, B., Skovsted, C., Steiner, M., Vendrasco, M., 2012. Chronology of early Cambrian biomineralization. Geol. Mag. 149, 221–251. https://doi.org/10.1017/s0016756811000720.

Luo, H.L., Jiang, Z.W., Tang, L.D., 1993. Discussion on the Douposi Formation. J. Stratigr. 17, 266–271. https://doi.org/10.19839/j.cnki.dcxzz.1993.04.003.

Matthew, G.F., 1899. Studies on Cambrian faunas, No. 3. Upper Cambrian fauna, Mount Stephen, British Columbia. The trilobites and worms. Trans. R. Soc. Can. 5, 39–66.

Merinero, R., Lunar, R., Martínez-Frías, J., Somoza, L., Díaz-del-Río, V., 2008. Iron oxyhydroxide and sulphide mineralization in hydrocarbon seep-related carbonate submarine chimneys, Gulf of Cadiz (SW Iberian Peninsula). Mar. Pet. Geol. 25, 706–713. https://doi.org/10.1016/j.marpetgeo.2008.03.005.

Palacios, T., Jensen, S., Sánchez, I.C., Mus, M.M., 2014. First lower Cambrian record of *Wiwaxia* from Northwest Gondwana: Small carbonaceous fossils from the Lancara Formation, Cantabrian Mountains, northern Spain. In: The Palaeontological Association 58th Annual Meeting. AGM papers, Programme Abstracts and.

Pedder, B.E., 2012. The Palynology and Stratigraphy of the Cambrian Nolichucky Shale and Associated Formations at Thorn Hill, Tennessee. Doctor of Philosophy University of Sheffield, USA.

Peng, S.C., 2020. Illustration of Cambrian Stratigraphy and Index Fossils of China: Trilobites. Zhejiang University Press, Hangzhou.

Porter, S.M., 2004. Halkieriids in Middle Cambrian phosphatic limestones from Australia. J. Paleontol. 78, 574–590. https://doi.org/10.1666/0022-3360(2004)078<0574:HIMCPL>2.0.CO;2.

Slater, B.J., Bohlin, M.S., 2022. Animal origins: the record from organic microfossils. Earth Sci. Rev. 232, 104107 https://doi.org/10.1016/j.earscirev.2022.104107.

Slater, B.J., Harvey, T.H.P., Guilbaud, R., Butterfield, N.J., Rahman, I., 2017. A cryptic record of Burgess Shale-type diversity from the early Cambrian of Baltica. Palaeontology 60, 117–140. https://doi.org/10.1111/pala.12273.

Smith, M.R., 2012. Mouthparts of the Burgess Shale fossils *Odontogriphus* and *Wiwaxia*: implications for the ancestral molluscan radula. Proc. R. Soc. Lond. B Biol. Sci. 279, 4287–4295. https://doi.org/10.1098/rspb.2012.1577.

Smith, M.R., 2014. Ontogeny, morphology and taxonomy of the soft-bodied Cambrian 'mollusc' *Wiwaxia*. Palaeontology 57, 215–229. https://doi.org/10.1111/pala.12063.

Smith, M.R., Hughes, G.M.G., Vargas, M.C., Parra, F.d.L., 2016. Sclerites and possible mouthparts of *Wiwaxia* from the temperate palaeolatitudes of Colombia, South America. Lethaia 49, 393–397. https://doi.org/10.1111/let.12154.

Sun, H.J., Zhao, Y.L., Peng, J., Yang, Y.N., 2014. New *Wiwaxia* material from the Tsinghsutung Formation (Cambrian Series 2) of Eastern Guizhou, China. Geol. Mag. 151, 339–348. https://doi.org/10.1017/s0016756813000216.

Swofford, D.L., 1998. PAUP*. Phylogenetic Analysis using Parsimony (*and Other Methods). Version 4 (Sinauer Associates).

Walcott, C.D., 1911. Middle Cambrian annelids. In: Walcott, C.D. (Ed.), Cambrian Geology and Palaeontology. The Smithsonian Institution, Washington, pp. 110–144.

Wei, H.Y., Wei, X.M., Qiu, Z., Song, H.Y., Shi, G., 2016. Redox conditions across the G–L boundary in South China: Evidence from pyrite morphology and sulfur isotopic compositions. Chem. Geol. 440, 1–14. https://doi.org/10.1016/j.chemgeo.2016.07.009.

Wilkin, R.T., Barnes, H.L., Brantley, S.L., 1996. The size distribution of framboidal pyrite in modern sediments: an indicator of redox conditions. Geochim. Cosmochim. Acta 60, 3897–3912. https://doi.org/10.1016/0016-7037(96)00209-8.

Wu, W., Yang, A., Janussen, D., Steiner, M., Zhu, M., 2005. Hexactinellid sponges from the early Cambrian black shale of South Anhui, China. J. Paleontol. 79, 1043–1051. https://doi.org/10.1666/00223360(2005)079[1043:HSFTEC]2.0.CO;2.

Xiang, L.W., Zhu, Z.L., Li, S.J., Zhou, Z.Q., 1999. Chinese Stratigraphic Lexicon (the Cambrian). Geological Publishing House, Beijing.

Xiao, S., Hu, J., Yuan, X., Parsley, R.L., Cao, R., 2005. Articulated sponges from the lower Cambrian Hetang Formation in southern Anhui, South China: their age and implications for the early evolution of sponges. Palaeogeogr. Palaeoclimatol. Palaeoecol. 220, 89–117. https://doi.org/10.1016/j.palaeo.2002.02.001.

Yang, X., Zhu, M., Zhao, Y., Wang, Y., 2005. Cambrian sponge assemblages from Guizhou. Acta Micropalaeontol. Sin. 44, 454–463. https://doi.org/10.3969/j.issn.1000-0674.2005.03.009.

Yang, J., Smith, M.R., Lan, T., Hou, J.B., Zhang, X.G., 2014. Articulated *Wiwaxia* from the Cambrian Stage 3 Xiaoshiba Lagerstätte. Sci. Rep. 4, 4643. https://doi.org/10.1038/srep04643.

Zhang, Z.F., Smith, M.R., Shu, D.G., 2015. New reconstruction of the *Wiwaxia* scleritome, with data from Chengjiang juveniles. Sci. Rep. 5, 14810. https://doi.org/10.1038/srep14810.

Zhao, Y.L., 2011. The Kaili Biota: Marine Organisms from 508 Million Years Ago. Guizhou Science and Technology Press, Guiyang.

Zhao, Y.L., Qian, Y., Li, S.X., 1994. *Wiwaxia* from Early-Middle Cambrian Kaili Formation in Taijiang, Guizhou. Acta Palaeontol. Sin. 33, 359–366. https://doi.org/10.19800/j.cnki.aps.1994.03.011.

Zhao, F.C., Smith Martin, R., Yin, Z.J., Zeng, H., Li, G.X., Zhu, M.Y., 2017. *Orthrozanclus elongata* n. sp. and the significance of sclerite-covered taxa for early trochozoan evolution. Sci. Rep. 7, 16232. https://doi.org/10.1038/s41598-017-16304-6.

Zhao, F.C., Smith, M.R., Yin, Z.J., Zeng, H., Hu, S.X., Li, G.X., Zhu, M.Y., 2015. First report of *Wiwaxia* from the Cambrian Chengjiang Lagerstätte. Geol. Mag. 152, 378–382. https://doi.org/10.1017/s0016756814000648.

Zhu, M.Y., Babcock, L.E., Steiner, M., 2005. Fossilization modes in the Chengjiang Lagerstätte (Cambrian of China): testing the roles of organic preservation and diagenetic alteration in exceptional preservation. Palaeogeogr. Palaeoclimatol. Palaeoecol. 220, 31–46. https://doi.org/10.1016/j.palaeo.2003.03.001.